Nanoscale Advances

ROYAL SOCIETY OF CHEMISTRY

PAPER

View Article Online
View Journal | View Issue

Cite this: *Nanoscale Adv.*, 2023, **5**, 479

Superconductivity in single-crystalline $ZrTe_{3-x}$ ($x \leq 0.5$) nanoplates†

Jie Wang, ‡[ab] Min Wu,‡*[a] Weili Zhen,[ab] Tian Li,[a] Yun Li,[ac] Xiangde Zhu,[a] Wei Ning*[a] and Mingliang Tian*[ad]

Received 15th September 2022
Accepted 17th November 2022

DOI: 10.1039/d2na00628f

rsc.li/nanoscale-advances

Superconductivity with an unusual filamented character below 2 K has been reported in bulk $ZrTe_3$ crystals, a well-known charge density wave (CDW) material, but still lacks in its nanostructures. Here, we systemically investigated the transport properties of controllable chemical vapor transport synthesized $ZrTe_{3-x}$ nanoplates. Intriguingly, superconducting behavior is found at $T_c = 3.4$ K and can be understood by the suppression of CDW due to the atomic disorder formed by Te vacancies. Magnetic field and angle dependent upper critical field revealed that the superconductivity in the nanoplates exhibits a large anisotropy and two-dimensional character. This two-dimensional nature of superconductivity was further satisfactorily described using the Berezinsky–Kosterlitz–Thouless transition. Our results not only demonstrate the critical role of Te vacancies for superconductivity in $ZrTe_{3-x}$ nanoplates, but also provide a promising platform to explore the exotic physics in the nanostructure devices.

Two-dimensional (2D) layered transition metal dichalcogenides (TMDs) have attracted extensive attention owing to their plethora of remarkable physical properties,[1–3] including superconductivity,[4–6] charge density wave (CDW),[7–9] Mott insulator,[10–12] topological phase,[13–15] moiré electronics *etc.*[16–19] Among the TMDs, zirconium tellurium compounds have attracted increasing research interest because of the existence of different compositions and properties. ZrTe was theoretically proposed to be a non-abelian topological semimetal with triply degenerate nodes,[20,21] and experimentally demonstrated to possess multiple Fermi surfaces with light effective masses by the measurement of quantum oscillations.[22] Massless Dirac fermions and negative magnetoresistance were observed in topological material candidate $ZrTe_2$.[23–25] Although the topological nature of $ZrTe_5$ remains a puzzle, a number of interesting phenomena have been discovered in transport experiments, such as log-periodic oscillations,[26] the quantum Hall effect,[27] four-fold splitting of the non-zero Landau levels,[28] gigantic magneto-chiral anisotropy,[29] *etc.* Another fascinating composition is layered $ZrTe_3$, which was known for decades as a CDW material.[30]

$ZrTe_3$ crystallizes in $TaSe_3$-type structure (space group $P2_1/m$), which consists of a quasi-one-dimensional chain along the *b*-axis and quasi-two-dimensional layer along the *ac* plane.[31] Electronically, a resistance anomaly associated with the formation of the CDW state due to Fermi surface nesting is established at 63 K in $ZrTe_3$ crystals.[30] More importantly, filamentary superconductivity below $T_c = 2$ K is observed at ambient pressure when the CDW is quenched.[32] To increase the superconducting transition temperature T_c, metal atom intercalation,[33] element substitution[34] and pressure[32] have been widely used. However, most studies on the superconductivity of $ZrTe_3$ were focused on the bulk crystals, and experimental evidence for the superconductivity in low-dimensional $ZrTe_3$ nanoplates or nanowires was rarely reported. Previous studies uncovered that the mechanically exfoliated $ZrTe_3$ nanowires display a semiconducting behavior,[35] and the $ZrTe_3$ nanoribbons prepared by chemical vapor deposition exhibit an unexpected ferromagnetism coming from structural imperfection and edge-states.[36] These observations limit the possibilities for unveiling the superconducting state in $ZrTe_3$ nanostructures. Therefore, whether the superconductivity survives in the $ZrTe_3$ nanostructures is still unknown.

In this work, we carried out comprehensive electrical transport measurements on chemical vapor transport (CVT) synthesized $ZrTe_{3-x}$ nanoplates, which were characterized by scanning electron microscopy (SEM), energy dispersive X-ray (EDX) spectroscopy and Raman spectroscopy. The $ZrTe_{3-x}$ nanoplates show a superconducting transition at $T_c = 3.4$ K, which was

[a]*Anhui Key Laboratory of Condensed Matter Physics at Extreme Conditions, High Magnetic Field Laboratory, HFIPS, Chinese Academy of Sciences, Hefei 230031, Anhui, P. R. China. E-mail: minwu@hmfl.ac.cn; ningwei@hmfl.ac.cn; tianml@hmfl.ac.cn*

[b]*Department of Physics, University of Science and Technology of China, Hefei 230026, P. R. China*

[c]*Department of Materials Science and Engineering, ARC Centre of Excellence in Future Low-Energy Electronics Technologies (FLEET), Monash University, Clayton, Victoria 3800, Australia*

[d]*Department of Physics, School of Physics and Materials Science, Anhui University, Hefei 230601, P. R. China*

† Electronic supplementary information (ESI) available. See DOI: https://doi.org/10.1039/d2na00628f

‡ These authors contributed equally to this work.

attributed to the existence of Te vacancies that are determined by using the EDX spectrum. Moreover, the superconducting behavior in $ZrTe_{3-x}$ nanoplates shows strong anisotropy with magnetic field orientation and 2D characteristics of that are consistent with the Berezinskii–Kosterlitz–Thouless (BKT) transition. Our results signify that $ZrTe_{3-x}$ nanoplates offer an opportunity for discovering novel phenomena in the nanostructure devices.

Usually, the chemical vapor deposition method was employed to grow high-quality nanoplates/nanowires of layered TMDs.[37] Very recently, it had been demonstrated that the CVT method also can be used to directly prepare thin flakes of TMDs with comparable quality by slowing down the growth rate.[38,39] Moreover, because of the CVT growth progress in an evacuated ampule, it is a useful way to grow ambient sensitive materials.[40] Thus, in this work, we utilized the CVT approach to synthesize the $ZrTe_3$ nanoplates in a neck ampule with iodine as a transport agent (to slow down the reaction rate, the ingredients are separated in the ampule), as shown in Fig. 1(a). 5 g Zr pieces and 100 mg I_2 were placed in an evacuated quartz tube, together with 0.3 g Te located at the position of the narrow neck of a quartz tube with a diameter of less than 1 cm. The evacuated ampule was placed into a horizontal two zone furnace, where the source zone was heated to 540 °C and the growth zone was heated to 450 °C at a rate of 1 °C per minute. After 150 minutes, the furnace was cooled down to room temperature. To study the transport properties, the grown $ZrTe_3$ nanoplates were transferred onto the conventional SiO_2/Si substrates in the glovebox, and then onto patterned electrodes by standard electron-beam lithography and lift-off techniques. To prevent contamination or oxidation, the devices were covered with poly (methyl methacrylate) layers on the surface before the transport measurements.

Fig. 1(b) shows the SEM image of the as-grown nanoplates on a pure silicon substrate, where most are rhombus or parallelogram shaped. However, when transferred onto SiO_2/Si substrates, the shapes of nanoplates changed into trapezoid (see the upper inset of Fig. 2(a)). The corresponding EDX data are shown in Fig. 1(c). Apparently, the nanoplates are composed of Zr and Te with an atomic ratio less than 1 : 3, indicating the presence of Te deficiencies in the nanoplates, and the stoichiometry should be $ZrTe_{3-x}$ ($x \leq 0.5$). Fig. 1(d) and (e) show the elemental mappings measured by EDX, from which Zr and Te atoms are uniformly distributed across the nanoplates. More structural characterizations (HRTEM and SAED) about $ZrTe_{3-x}$ nanoplates can be seen in the ESI Fig. S1.† The typical Raman spectra of synthesized $ZrTe_{3-x}$ nanoplates are shown in Fig. 1(f). Four obvious Raman peaks are found at $\omega_1 = 83\ cm^{-1}$, $\omega_2 = 106\ cm^{-1}$, $\omega_3 = 141\ cm^{-1}$, and $\omega_4 = 212\ cm^{-1}$, which are consistent with the previous reports.[31,33]

Fig. 2(a) shows the temperature dependence of nanoplate resistance under a zero magnetic field. Metallic behavior was observed above 4.5 K, below which the resistance begins to decrease and it drops to zero at 2.3 K (as indicated by the enlarged $R(T)$ curve in the bottom inset of Fig. 2(a)), indicating the occurrence of a superconducting transition in $ZrTe_{3-x}$ nanoplates. To quantitatively analyze the superconductivity, the "50% criterion" was used to define T_c (upper critical field B_c) as the temperature (magnetic field) at which the resistance drops to 50% of the normal state value. In this case, T_c is about 3.4 K, which is larger than that of bulk $ZrTe_3$ crystals.[28] Superconductivity transport of different samples can be seen from ESI

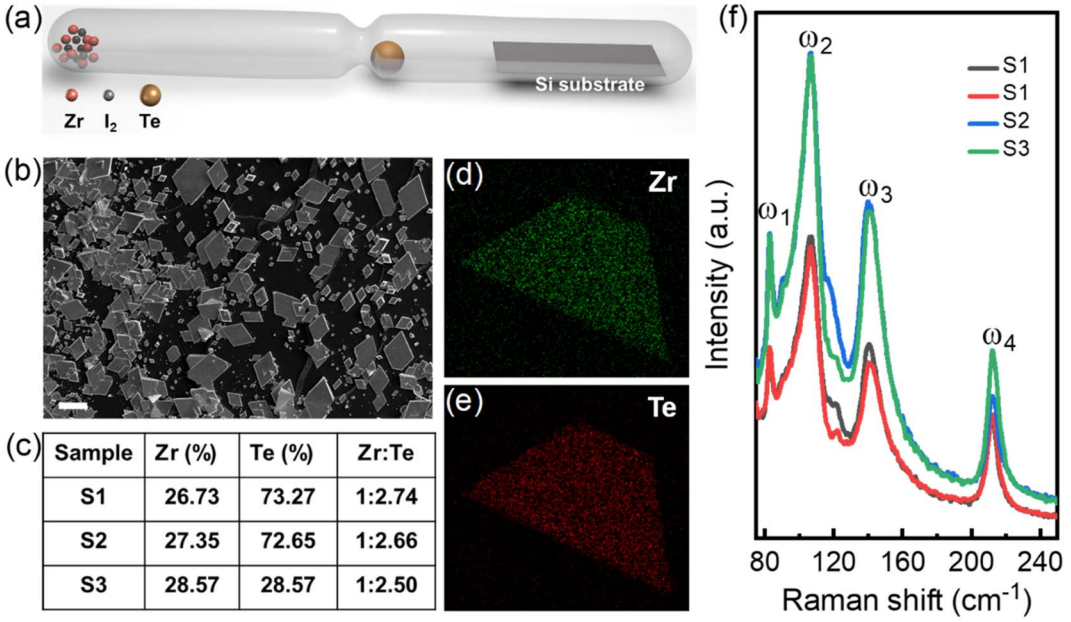

Sample	Zr (%)	Te (%)	Zr:Te
S1	26.73	73.27	1:2.74
S2	27.35	72.65	1:2.66
S3	28.57	28.57	1:2.50

Fig. 1 Synthesis and characterization of $ZrTe_{3-x}$ nanoplates. (a) Schematic for growing $ZrTe_{3-x}$ nanoplates by the controlled CVT method. (b) SEM image of as-grown $ZrTe_{3-x}$ nanoplates on pure silicon. Scale bars: 20 μm. (c) The chemical element ratio of the three samples. (c) Atomic ratio of the nanoplates determined by using the EDX spectrum. (d and e) Mapping images of Zr and Te elements, respectively. (f) Raman spectrum of $ZrTe_{3-x}$ nanoplates.

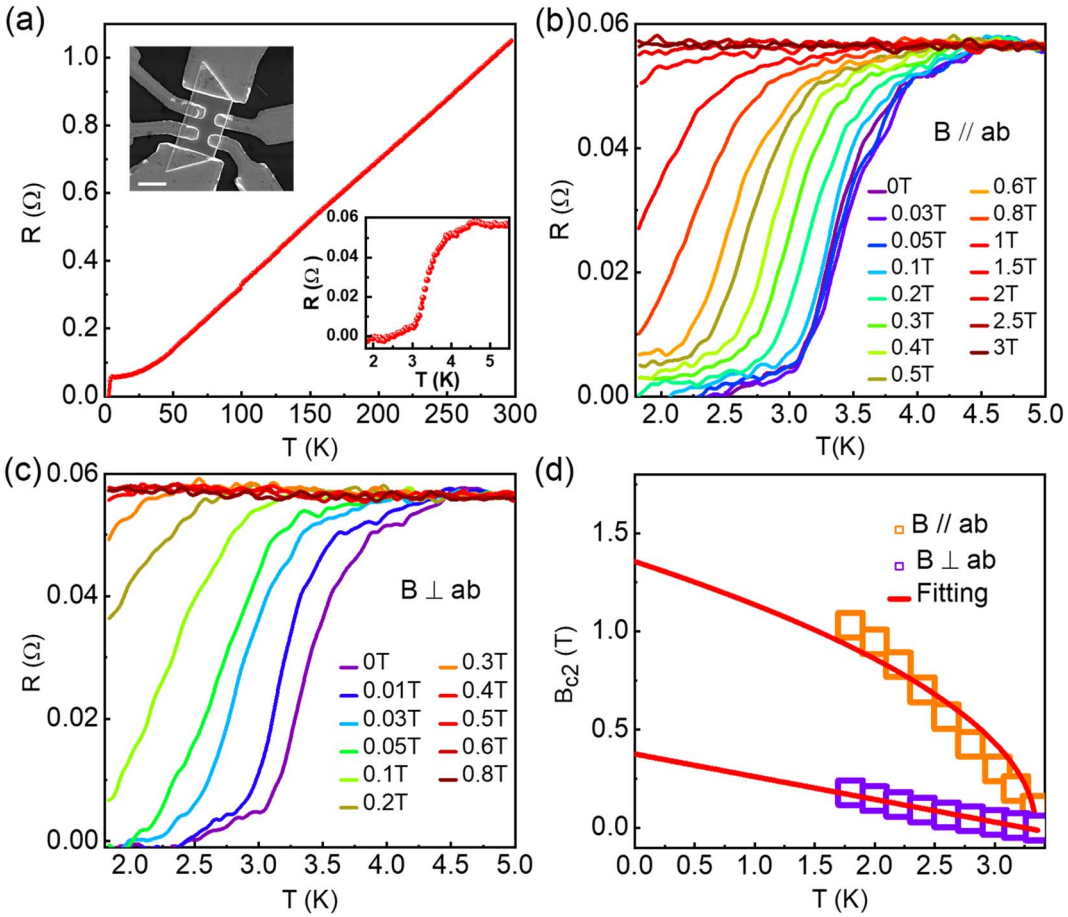

Fig. 2 Anisotropic superconducting behavior in $ZrTe_{3-x}$ nanoplates. (a) Temperature dependence of resistance. Upper inset: SEM image of a typical device. Bottom inset: Enlarged $R-T$ curve around the superconductivity critical temperature. (b and c) The temperature-dependent resistance under a magnetic field parallel to and perpendicular to the sample plane, respectively. (d) Temperature-dependent B_{c2} for the magnetic field parallel to and perpendicular to the sample plane with the red curves showing the theoretical fitting by the standard GL model.

Fig. S2–S5.† Previous studies have demonstrated that high growth temperature and doping can enhance the superconducting transition temperature T_c of bulk $ZrTe_3$ through inducing disorders that suppress the CDW state.[34,41] Superconductivity and charge density waves are in significant competition and the existence of charge density waves is detrimental to superconductivity. In our samples, by introducing appropriate tellurium vacancies, we found that the charge density wave was significantly suppressed and the superconductivity emerged during transport measurements, which is consistent with previous results, such as element substitution, intercalation and high pressure. Therefore, we conclude that the observed superconductivity with higher T_c in $ZrTe_{3-x}$ nanoplates can be ascribed to the presence of Te vacancies determined from the EDX spectrometry (Fig. 1(c) and ESI Table S1†).

To study the anisotropy of superconductivity in $ZrTe_{3-x}$ nanoplates, we investigated the temperature dependence of resistance when different magnetic fields are parallel and perpendicular to the sample plane and the results are presented in Fig. 2(b) and (c). In both configurations, the superconducting transition temperature shifts to a lower temperature with the increase in the magnetic field. The magnetic field that completely suppresses the superconductivity is about 2.5 T for the parallel field direction ($B\|$ab), which is 5 times larger than that for the perpendicular scenario ($B\perp$ab, ~0.5 T). The large anisotropy of the upper critical field indicates 2D characteristics of superconductivity in $ZrTe_{3-x}$ nanoplates. In addition, the dependence of the out-of-plane upper critical field on a temperature close to T_c displays a linear behavior, as shown in Fig. 2(d), which is in accordance with the standard Ginzburg–Landau (GL) theory:[42]

$$B_{c2,\perp}(T) = \frac{\Phi_0}{2\pi\xi_{GL}(0)^2}\left(1-\frac{T}{T_c}\right) \quad (1)$$

where Φ_0 and $\xi_{GL}(0)$ are the flux quantum and GL coherence length, respectively. The estimated GL coherence length from the fitting curve (Fig. 2(d)) is about 29.6 nm. For the in-plane field scenario, the temperature dependence of the upper critical field follows the 2D GL behavior:[43]

$$B_{c2,\|}(T) = \frac{\Phi_0\sqrt{12}}{2\pi\xi_{GL}(0)d_{sc}}\left(1-\frac{T}{T_c}\right)^{1/2} \quad (2)$$

where d_{sc} is the superconducting thickness. As depicted in Fig. 2(d), the extracted d_{sc} is about 28.4 nm and smaller than the GL coherence length, which is consistent with the expectation for a 2D superconductor.

To further uncover the dimensionality of superconductivity in $ZrTe_{3-x}$ nanoplates, we performed the angle dependent superconducting transition measurements. Fig. 3(a) shows the magnetic field direction dependence of nanoplate resistance at $T = 1.8$ K, where θ is the tilted angle between the direction of current and magnetic field B, as schematically illustrated in the inset of Fig. 3(a). With decreasing angle θ, the superconducting transition shifts to a high magnetic field and the upper critical field reaches a maximum at $\theta = 0°$ (Fig. 3(b)). It has been verified that the upper critical field in a 2D superconductor is significantly enhanced when the magnetic field is parallel to the sample plane,[44] which is consistent with our results, as shown in Fig. 3. Furthermore, the relationship between θ and upper critical field B_{c2} exhibits a sharp cusp, as plotted and shown in Fig. 3(b). All these experimental pieces of evidence enable us to deduce that the observed superconductivity in $ZrTe_{3-x}$ nanoplates has a 2D nature. For a superconductor with 2D characteristics, the angle dependent B_{c2} can be well described by using the Thinkham model:[44,45].

$$\left|\frac{B_{c2}(\theta)\sin\theta}{B_{c2,\perp}}\right| + \left(\frac{B_{c2}(\theta)\cos\theta}{B_{c2,\parallel}}\right)^2 = 1 \lim_{x\to\infty} \quad (3)$$

As indicated by the red solid curve in the inset of Fig. 3(b), the experimental data can be well captured by using the Thinkham model. It is worth pointing out that the 3D anisotropic GL model[46] is also utilized to fit $B_{c2}(\theta)$, as indicated by the blue solid curve in the inset of Fig. 3(b). Obviously, the fitting cannot describe the $B_{c2}(\theta)$ curve.

It is well known that the transport properties for 2D characteristic superconductivity feature a BKT transition that is characterized by the BKT temperature T_{BKT}.[47] Fig. 4(a) shows the I–V curves on a log–log scale with temperature ranging from 2.4 K to 4.6 K. The V–I dependence is found to obey a power-law, $V \propto I^{\alpha}$, and α represents slopes of the curve when the current approaches the linear region. The linear line has a slope of 1 in the high temperature region (4.4–4.6 K), which means the complete disappearance of superconductivity. The dashed line corresponds to $V \propto I^3$ at the BKT transition. The temperature dependence of the exponent α is shown in Fig. 4(b). It can be seen that the value of α increases rapidly with $T < T_c$, and approaches 3 at a temperature of ~3.17 K, which is thus identified as T_{BKT}. In addition, according to the BKT model, the $R(T)$ curve under a zero magnetic field at just above T_{BKT} follows the Halperin–Nelson equation:[42]

$$R = R_0 \exp\left(-bt^{-\frac{1}{2}}\right) \quad (4)$$

where R_0 and b are material-specific parameters, and $t = \frac{T}{T_{BKT}} - 1$ As shown in Fig. 4(c), the $R(T)$ data can be well fitted by using eqn (3), yielding $T_{BKT} = 3.16$ K, which is highly consistent with the value obtained from the power-law analysis of the I–V curves. The existence of the BKT transition provides further strong evidence for the 2D nature of superconductivity in $ZrTe_{3-x}$ nanoplates.

In conclusion, we have presented systematic transport properties of CVT grown $ZrTe_{3-x}$ nanoplates. The superconducting transition is found at $T = 3.4$ K due to the existence of Te vacancies in the nanoplates, as revealed by the EDX spectrum. Meanwhile, the observed superconductivity exhibits large anisotropy with the magnetic field direction and features the 2D nature of the superconducting transition that was demonstrated by the existence of the BKT transition. Our results suggest thin flakes of layered TMDs prepared by CVT provide a viable way to study the potential properties in the nanostructures.

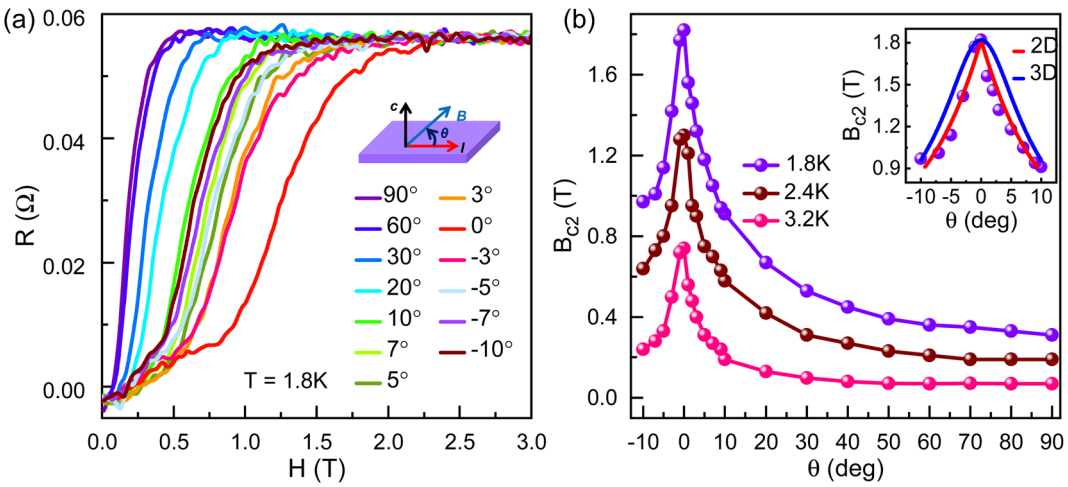

Fig. 3 Angular dependence of transport properties in $ZrTe_{3-x}$ nanoplates. (a) Resistance as a function of magnetic field at different angles measured at $T = 1.8$ K. Inset: Schematic of angular-dependent resistance measurement. (b) Angle-dependent upper critical field B_c measured at $T = 1.8$ K, 2.4 K, and 3.2 K. Inset: Comparation between the Thinkham model (red line) and GL model (blue line) within ±10.

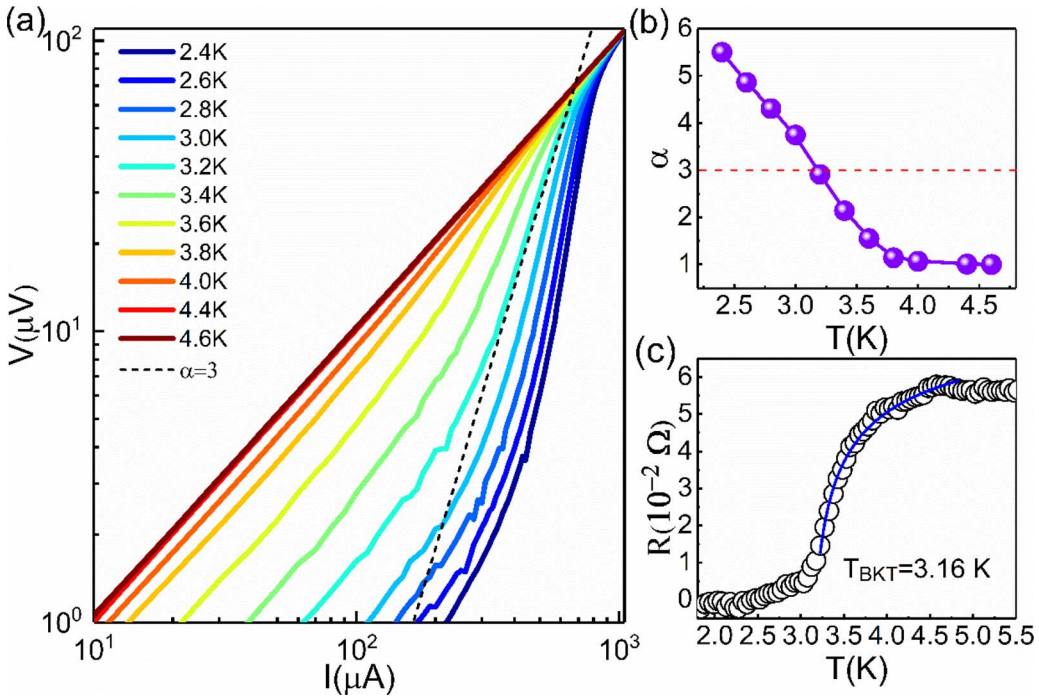

Fig. 4 The BKT transition in $ZrTe_{3-x}$ nanoplates. (a) Voltage dependence of current from 2.4 K to 4.6 K. The dashed line corresponds to $V \propto I^3$. (b) Temperature dependence of the exponent α extracted from V–I curves in (a). The BKT temperature is about $T_{BKT} = 3.17$ K as indicated by the dashed line. (c) At $B = 0$, the $R(T)$ curve can be well fitted by using the Halperin–Nelson formula above T_{BKT}, which yields $T_{BKT} = 3.16$ K.

Data availability

The data that support the findings of this study are available from the corresponding author upon reasonable request.

Conflicts of interest

The authors have no conflicts of interests.

Acknowledgements

This work was supported by the National Key Research and Development Program of China (Grant No. 2021YFA1600201) and the Natural Science Foundation of China (No. U19A2093, U2032214, and U2032163)

References

1 L. F. Gao, C. Y. Ma, S. R. Wei, A. V. Kuklin, H. Zhang and H. Agren, *ACS Nano*, 2021, **15**, 954–965.
2 Y. Zhang, P. Huang, J. Guo, R. C. Shi, W. C. Huang, Z. Shi, L. M. Wu, F. Zhang, L. F. Gao, C. Li, X. W. Zhang, J. L. Xu and H. Zhang, *Adv. Mater.*, 2020, **32**, 2001082.
3 H. Qiao, Z. Y. Huang, X. H. Ren, S. H. Liu, Y. P. Zhang, X. Qi and H. Zhang, *Adv. Opt. Mater.*, 2020, **8**, 1900765.
4 X. X. Xi, Z. F. Wang, W. W. Zhao, J. H. Park, K. T. Law, H. Berger, L. Forro, J. Shan and K. F. Mak, *Nat. Phys.*, 2016, **12**, 139–143.
5 J. M. Lu, O. Zheliuk, I. Leermakers, N. F. Q. Yuan, K. T. Law and J. T. Ye, *Science*, 2015, **350**, 1353–1357.
6 W. Shi, J. T. Ye, Y. J. Zhang, R. Suzuki, M. Yoshida, J. Miyazaki, N. Inoue, Y. Saito and Y. Iwasa, *Science*, 2015, **5**, 12534.
7 Y. J. Yu, F. Y. Yang, L. F. Lu, Y. J. Yan, Y. H. Cho, L. G. Ma, X. H. Niu, S. Kim, Y. W. Son, D. L. Feng, S. Y. Li, S. W. Cheong, X. H. Chen and Y. B. Zhang, *Nat. Nanotechnol.*, 2015, **10**, 270–276.
8 X. D. Zhu, H. C. Lei and C. Petrovic, *Phys. Rev. Lett.*, 2011, **106**, 246404.
9 Y. K. Nakata, K. Sugawara, A. Chainani, H. Oka, C. H. Bao, S. H. Zhou, P. Y. Chuang, C. M. Cheng, T. Kawakami, Y. Saruta, T. Fukumura, S. Y. Zhou, T. Takahashi and T. Sato, *Nat. Commun.*, 2021, **12**, 5873.
10 Y. Nakata, K. Sugawara, R. Shimizu, Y. Okada, P. Han, T. Hitosugi, K. Ueno, T. Sato and T. Takahashi, *NPG Asia Mater.*, 2016, **8**, e321.
11 Y. Nakata, T. Yoshizawa, K. Sugawara, Y. Umemoto, T. Takahashi and T. Sato, *ACS Appl. Nano Mater.*, 2018, **1**, 1456–1460.
12 B. H. Moon, J. J. Bae, M. K. Joo, H. Choi, G. H. Han, H. Lim and Y. H. Lee, *Nat. Commun.*, 2018, **9**, 2052.
13 J. Xia, D. F. Li, J. D. Zhou, P. Yu, J. H. Lin, J. L. Kuo, H. B. Li, Z. Liu, J. X. Yan and Z. X. Shen, *Small*, 2017, **13**, 1701887.
14 F. Leonard, W. L. Yu, K. C. Collins, D. L. Medlin, J. D. Sugar, A. A. Talin and W. Pan, *ACS Appl. Mater. Interfaces*, 2017, **9**, 37041–37047.
15 Q. Q. Liu, F. C. Fei, B. Chen, X. Y. Bo, B. Y. Wei, S. Zhang, M. H. Zhang, F. J. Xie, M. Naveed, X. G. Wan, F. Q. Song and B. G. Wang, *Phys. Rev. B*, 2019, **99**, 155119.

16 C. H. Jin, Z. Tao, T. X. Li, Y. Xu, Y. H. Tang, J. C. Zhu, S. Liu, K. J. Watanabe, T. Taniguchi, J. C. Hone, L. Fu, J. Shan and K. F. Mak, *Nat. Mater.*, 2022, **20**, 940–944.
17 Y. Xu, S. Liu, D. A. Rhodes, K. J. Watanabe, T. Taniguchi, J. Hone, V. Elser, K. F. Mak and J. Shan, *Nature*, 2020, **587**, 214–218.
18 Y. H. Tang, L. Z. Li, T. X. Li, Y. Xu, S. Liu, K. Barmak, K. J. Watanabe, T. Taniguchi, A. H. MacDonald, J. Shan and K. F. Mak, *Nature*, 2020, **579**, 353–358.
19 L. Wang, E. M. Shih, A. Ghiotto, L. D. Xian, D. A. Rhodes, C. Tan, M. Claassen, D. M. Kennes, Y. S. Bai, B. Kim, K. J. Watanabe, T. Taniguchi, X. Y. Zhu, J. Hone, A. Rubio, A. N. Pasupathy and C. R. Dean, *Nat. Mater.*, 2020, **19**, 861–866.
20 H. M. Weng, C. Fang, Z. Fang and X. Dai, *Phys. Rev. B*, 2016, **94**, 165201.
21 A. Bouhon, Q. S. Wu, R. J. Slager, H. M. Weng, O. V. Yazyev and T. Bzdusek, *Nat. Phys.*, 2020, **16**, 1137–1143.
22 W. L. Zhu, J. B. He, Y. J. Xu, S. Zhang, D. Chen, L. Shan, Y. F. Yang, Z. A. Ren, G. Li and G. F. Chen, *Phys. Rev. B*, 2020, **101**, 245127.
23 P. Tsipas, D. Tsoutsou, S. Fragkos, R. Sant, C. Alvarez, H. Okuno, G. Renaud, R. Alcotte, T. Baron and A. Dimoulas, *ACS Nano*, 2018, **12**, 1696–1703.
24 H. C. Wang, C. H. Chan, C. H. Suen, S. P. Lau and J. Y. Dai, *ACS Nano*, 2019, **13**, 6008–6016.
25 J. Wang, Y. H. Wang, M. Wu, J. B. Li, S. P. Miao, Q. Y. Hou, Y. Li, J. H. Zhou, X. D. Zhu, Y. M. Xiong, W. Ning and M. L. Tian, *Appl. Phys. Lett.*, 2022, **120**, 163103.
26 H. H. Wang, H. W. Liu, Y. N. Li, Y. J. Liu, J. F. Wang, J. Liu, J. Y. Dai, Y. Wang, L. Li, J. Q. Yan, D. Mandrus, X. C. Xie and J. Wang, *Sci. Adv.*, 2018, **4**, eaau5096.
27 F. D. Tang, Y. F. Ren, P. P. Wang, R. D. Zhong, J. Schneeloch, S. Y. Yang, K. Yang, P. A. Lee, G. D. Gu, Z. H. Qiao and L. Y. Zhang, *Nature*, 2021, **569**, 537–541.
28 J. Y. Wang, Y. X. Jiang, T. H. Zhao, Z. L. Dun, A. L. Miettinen, X. S. Wu, M. Mourigal, H. D. Zhou, W. Pan, D. Smirnov and Z. G. Jiang, *Nat. Commun.*, 2021, **12**, 6758.
29 Y. J. Wang, H. F. Legg, T. Bomerich, J. H. Park, S. Biesenkamp, A. A. Taskin, M. Braden, A. Rosch and Y. C. Ando, *Phys. Rev. Lett.*, 2022, **128**, 176602.
30 M. Hoesch, X. Y. Cui, K. Y. Shimada, C. Battaglia, S. I. Fujimori and H. Berger, *Phys. Rev. B*, 2009, **80**, 075423.
31 S. L. Gleason, Y. Gim, T. Byrum, A. Kogar, P. Abbamonte, E. Fradkin, G. J. MacDougall, D. J. Van Harlingen, X. D. Zhu, C. Petrovic and S. L. Cooper, *Phys. Rev. B*, 2015, **91**, 155124.
32 K. M. Gu, R. A. Susilo, F. Ke, W. Deng, Y. J. Wang, L. K. Zhang, H. Xiao and B. Chen, *J. Phys.: Condens. Matter*, 2018, **30**, 385701.
33 X. D. Zhu, H. C. Lei and C. Petrovic, *Phys. Rev. Lett.*, 2011, **106**, 246404.
34 X. D. Zhu, W. Ning, L. J. Li, L. S. Ling, R. R. Zhang, J. L. Zhang, K. F. Wang, Y. Liu, L. Pi, Y. C. Ma, H. F. Du, M. L. Min, Y. P. Sun, C. Petrovic and Y. H. Zhang, *Sci. Rep.*, 2016, **6**, 26974.
35 A. Geremew, M. A. Bloodgood, E. Aytan, B. W. K. Woo, S. R. Corber, G. Liu, K. Bozhilov, T. T. Salguero, S. Rumyantev, M. P. Rao and A. A. Balandin, *IEEE*, 2018, **39**, 735–738.
36 X. Yu, X. K. Wen, W. F. Zhang, L. Yang, H. Wu, X. Lou, Z. J. Xie, Y. Liu and H. X. Chang, *CrystEngCom*, 2019, **21**, 5586–5594.
37 B. J. Tang, X. W. Wang, M. J. Han, X. D. Xu, Z. W. Zhang, C. Zhu, X. Cao, Y. M. Yang, Q. D. Fu, J. Q. Yang, X. J. Li, W. B. Gao, J. D. Zhou, J. H. Lin and Z. Liu, *Nat. Electron.*, 2022, **5**, 224–232.
38 J. Y. Wang, H. S. Zheng, G. C. Xu, L. F. Sun, D. K. Hu, Z. X. Lu, L. Liu, J. Y. Zheng, C. G. Tao and L. Y. Jiao, *J. Am. Chem. Soc.*, 2016, **138**, 16216–16219.
39 K. Yuan, R. Y. Yin, X. Q. Li, Y. M. Han, M. Wu, S. L. Chen, S. Liu, X. L. Xu, K. J. Watanabe, T. Taniguchi, D. A. Muller, J. J. Shi, P. Gao, X. S. Wu, Y. Ye and L. Dai, *Adv. Funct. Mater.*, 2019, **29**, 1904032.
40 D. K. Hu, G. C. Xu, L. Xing, X. X. Yan, J. Y. Wang, J. Y. Zheng, Z. X. Lu, P. Wang, X. Q. Pan and L. Y. Jiao, *Angew. Chem., Int. Ed.*, 2017, **56**, 3611–3615.
41 X. Y. Zhu, B. Lv, F. Y. Wei, X. Y. Xue, B. Lorenz, L. Z. Deng, Y. Y. Sun and C. W. Chu, *Phys. Rev. B*, 2013, **87**, 024508.
42 C. Xu, L. B. Wang, Z. B. Liu, L. Chen, J. K. Guo, N. Kang, X. L. Ma, H. M. Cheng and W. C. Ren, *Nat. Mater.*, 2015, **14**, 1135–1141.
43 P. Baidya, D. Sahani, H. K. Kundu, S. Kaur, P. Tiwari, V. Bagwe, J. Jesudasan, A. Narayan, P. Raychaudhuri and A. Bid, *Phys. Rev. B*, 2021, **104**, 174510.
44 J. W. Zeng, E. F. Liu, Y. J. Fu, Z. Y. Chen, C. Pan, C. Y. Wang, M. Wang, Y. J. Wang, K. Xu, S. H. Cai, X. X. Yan, Y. Wang, X. W. Liu, P. Wang, S. J. Liang, Y. Cui, H. Y. Hwang, H. T. Yuan and F. Miao, *Nano Lett.*, 2018, **18**, 1410–1415.
45 Y. C. Zou, Z. G. Chen, E. Z. Zhang, F. X. Xiu, S. Matsumura, L. Yang, M. Hong and J. Zou, *Nanoscale*, 2017, **9**, 16591.
46 Y. T. Chan, P. L. Alireza, K. Y. Yip, Q. Niu, K. T. Lai and S. K. Goh, *Phys. Rev. B*, 2017, **96**, 180504.
47 Q. L. He, H. C. Liu, M. Q. He, Y. H. Lai, H. T. He, G. Wang, K. T. Law, R. Lortz, J. N. Wang and I. K. Sou, *Nat. Commun.*, 2014, **5**, 4247.